

Communication

New carbazole-substituted siloles for the fabrication of efficient non-doped OLEDs

Yi Xiong^a, Jiajie Zeng^a, Bin Chen^a, Jacky W.Y. Lam^c, Zujin Zhao^{a,*}, Shuming Chen^{b,*}, Ben Zhong Tang^{a,c,**}^a State Key Laboratory of Luminescent Materials and Devices, Center for Aggregation-Induced Emission, South China University of Technology, Guangzhou 510640, China^b Department of Electrical and Electronic Engineering, South University of Science and Technology of China, Shenzhen 518055, China^c Department of Chemistry, Hong Kong Branch of Chinese National Engineering Research Center for Tissue Restoration and Reconstruction, The Hong Kong University of Science & Technology, Hong Kong, China

ARTICLE INFO

Article history:

Received 12 November 2018

Received in revised form 2 December 2018

Accepted 18 December 2018

Available online 21 December 2018

Keywords:

Aggregation-induced emission

Silole

Photoluminescence

Electroluminescence

Organic light-emitting diode

ABSTRACT

Luminogenic molecules with aggregation-induced emission (AIE) property are free of aggregation-caused quenching and thus have great potential in the fabrication of efficient non-doped OLEDs. Herein, a series of new carbazole-substituted siloles have been synthesized and characterized. Their crystal and electronic structures, thermal stabilities, electrochemical behaviors, and photophysical properties are thoroughly investigated. These silole derivatives exhibit prominent AIE characteristics with high emission efficiencies in solid films. They can function as light-emitting layers in non-doped OLEDs, affording eminent electroluminescence efficiencies of 17.59 cd/A, 12.55 lm/W and 5.63%, amongst the most efficient non-doped OLEDs based on fluorescent emitters, indicating their promising applications in OLEDs.

© 2018 Chinese Chemical Society and Institute of Materia Medica, Chinese Academy of Medical Sciences.

Published by Elsevier B.V. All rights reserved.

In recent decades, tremendous progresses have been achieved in the development of optoelectronic devices [1]. One of the most promising optoelectronic devices is organic light-emitting diode (OLED), whose response time and contrast ratio can be even better than liquid crystal display [2]. The key active materials for OLEDs are the organic luminescent materials, one important kind of organic semiconductors. The studies on the preparation and application for them have got considerable attentions around the world [3]. Since organic luminescent materials are applied as solid films in OLEDs, their solid-state emission efficiencies are of significant importance to the performances of OLEDs. However, there is still a thorny issue of aggregation-caused quenching (ACQ) of conventional chromophores [4], that is the emissions of these chromophores are weakened or totally quenched in the aggregated state, even if they can emit strongly in the solution state. In general, a vast majority of the conventional organic luminescent materials

have a large and extended conjugated plane, which makes them prone to experience serious intermolecular interactions, and thus quenches the emissions in the aggregated state. Although multifarious chemical and engineering methods have been utilized for surmounting the ACQ problem, the attempts meet with only a limited success [5]. Thus, the exploration of organic luminescent materials with strong emissions in the aggregated state for the application in OLEDs remains as an important research topic.

Aggregation-induced emission (AIE), a unique phenomenon opposite to ACQ, has evoked intense academic and industrial interest. The luminogens with AIE property (AIEgens) are almost non-fluorescent in dilute solutions but can emit strongly in aggregates or solid films, furnishing an effective approach to solve the ACQ problem [6]. In order to figure out the inner connections between the molecular structures and properties of AIEgens, several of meaningful experiments and calculations have been conducted. And exploiting more practical applications and deciphering the working mechanism for AIEgens are also of high importance. Currently, the mostly accepted theory about the AIE mechanism is restriction of intramolecular motions (RIM), including rotation, vibration, twisting, stretching, etc. [7]. The active intramolecular motions in solutions can nonradiatively deactivate the excited state, but in the aggregated state, these

* Corresponding authors.

** Corresponding author at: Department of Chemistry, Hong Kong Branch of Chinese National Engineering Research Center for Tissue Restoration and Reconstruction, The Hong Kong University of Science & Technology, Hong Kong, China.

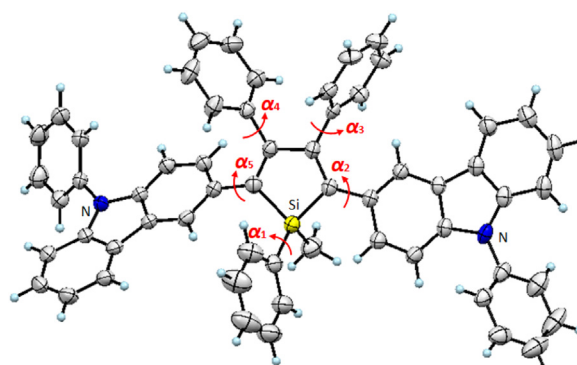
E-mail addresses: mszjzhao@scut.edu.cn (Z. Zhao), chen.sm@sustc.edu.cn (S. Chen), tangbenz@ust.hk (B.Z. Tang).

motions are greatly suppressed by physical constraint as well as weak intermolecular interactions, such as C–H··· π hydron bonds. In consequence, the nonradiative decay channel is blocked, and thus the excited state energy can dissipate *via* radiative transition, rendering greatly enhanced emissions [8].

Siloles are created with high electron affinity and fast electron mobility because of their unique $\sigma^*-\pi^*$ conjugated electronic structures, while the exceptional propeller-like molecular structures can bring about distinguished photophysical property of AIE [9]. Consequently, they are widely adopted as effective building units to construct various functional materials for optoelectronic devices with excellent performances [10,11]. In this work, we have prepared three new silole derivatives by combining 1-methyl-1,3,4-triphenyl-1*H*-silole and electron-donating 9-phenyl-9*H*-carbazole *via* different manners (Fig. 1). These silole derivatives possess distinct AIE characteristic and can fluoresce strongly in solid films. The non-doped OLEDs with excellent electroluminescence (EL) efficiencies have been fabricated based on these silole derivatives.

The target compounds 2,2'-MTPS-CaP, 3,3'-MTPS-CaP and 9,9'-MTPS-CaP were synthesized according to the synthetic routes illustrated in Scheme S1 in Supporting information. These new silole derivatives were yellow solids, and for them, THF, dichloromethane and toluene are good solvents, but water and ethanol are poor solvents. For the study and application in OLEDs, their thermal stability was evaluated. Thermogravimetric analysis (TGA) was carried out under nitrogen atmosphere at a heating rate of 10 °C/min, and high decomposition temperatures (T_d), corresponding to 5% initial weight loss, of 433.8, 452.4 and 440.8 °C for 2,2'-MTPS-CaP, 3,3'-MTPS-CaP and 9,9'-MTPS-CaP, respectively, were recorded (Fig. S1A in Supporting information), indicating they are thermally stable enough for film preparation by vacuum deposition. In addition, high glass-transition temperatures (T_g) of 133.4, 147.1 and 136.2 °C were also detected (Fig. S1B), revealing these compounds are morphological stable, which are conducive to the stability of the devices.

Crystal structure can provide useful information about the spatial conformation and stacking mode of the compounds in the aggregated state. Single crystals of 3,3'-MTPS-CaP were grown from CH₂Cl₂-C₂H₅OH mixture, and analyzed by X-ray diffraction crystallography. According to the crystal structure depicted in Fig. 2, 3,3'-MTPS-CaP shows a highly twisted conformation, and the dihedral angles between phenyls and the silole core at the 1,3,4-positions are 67.99°, 82.55° and 80.01°, respectively. In addition, the two substituents at 2,5-positions are unsymmetrical, where the dihedral angles between carbazoles and silole core at these two positions are 47.83° and 9.39°, respectively. Further analysis for packing pattern of 3,3'-MTPS-CaP indicates that there are multiple intramolecular and intermolecular C–H··· π hydrogen bonds within the range of 2.648–3.039 Å (Fig. S2 in Supporting information). These weak interactions will rigidify molecular structure and restrict the intramolecular motions in the solid state. However, no $\pi-\pi$ stacking interactions in crystalline state of 3,3'-MTPS-CaP are found. A highly twisted conformation is helpful to



$$\alpha_1 = 80.01^\circ, \alpha_2 = 9.39^\circ, \alpha_3 = 82.55^\circ, \alpha_4 = 67.99^\circ \text{ and } \alpha_5 = 47.83^\circ$$

Fig. 2. ORTEP drawing of the crystal structure of 3,3'-MTPS-CaP.

prevent strong intermolecular $\pi-\pi$ interaction, and suppress the emission quenching in the condensed phase.

The absorption maxima of 2,2'-MTPS-CaP, 3,3'-MTPS-CaP and 9,9'-MTPS-CaP in dilute THF solution (10^{-5} mol/L) are located at 398, 404 and 385 nm, owing to the $\pi-\pi^*$ electron transition (Fig. 3A). The optical band gaps of 2,2'-MTPS-CaP and 3,3'-MTPS-CaP are relatively narrower than that of 9,9'-MTPS-CaP, estimated from the onset of absorption spectra, which indicate that 2,2'-MTPS-CaP and 3,3'-MTPS-CaP have better effective conjugation than 9,9'-MTPS-CaP. The photoluminescence (PL) emissions of 2,2'-MTPS-CaP, 3,3'-MTPS-CaP and 9,9'-MTPS-CaP in dilute THF solutions are very weak, with PL peaks at 525, 526 and 520 nm, and low Φ_{FS} of 5.75%, 4.00% and 3.20%, respectively. After fabricated into solid films, they present slightly red-shifted and greatly enhanced PL peaks within the range of 520–539 nm (Fig. 3B). Their Φ_{FS} are significantly increased to 69.93%, 60.33% and 80.00% (Table 1), indicating their AIE characteristics. To further assess the PL properties of 2,2'-MTPS-CaP, 3,3'-MTPS-CaP and 9,9'-MTPS-CaP, the fluorescence lifetimes (τ), important parameters used to describe the excited-state decay processes, were measured and fitted. The intersystem crossing (ISC) process had been ignored in the excited-state decay process of silole derivatives because of

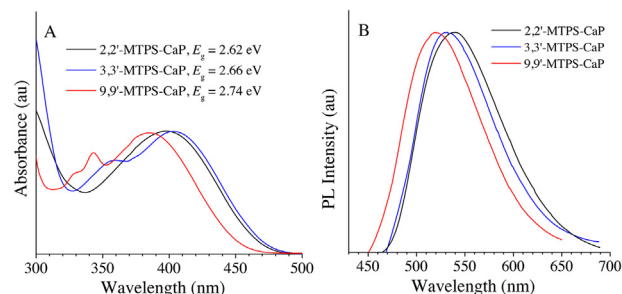


Fig. 3. (A) Absorption spectra in THF solutions, (B) photoluminescence (PL) spectra in solid films of these new silole derivatives. E_g = optical band gap.

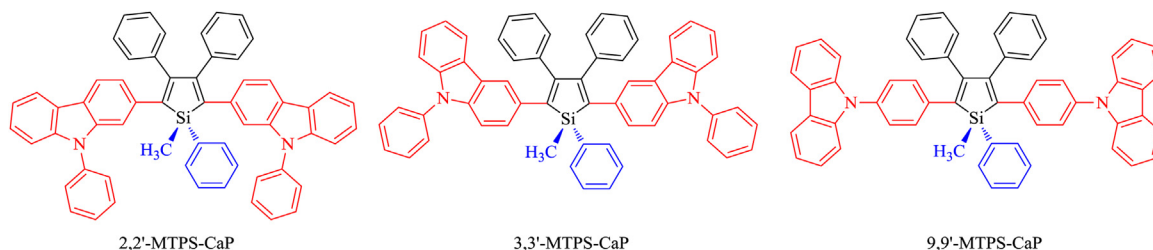
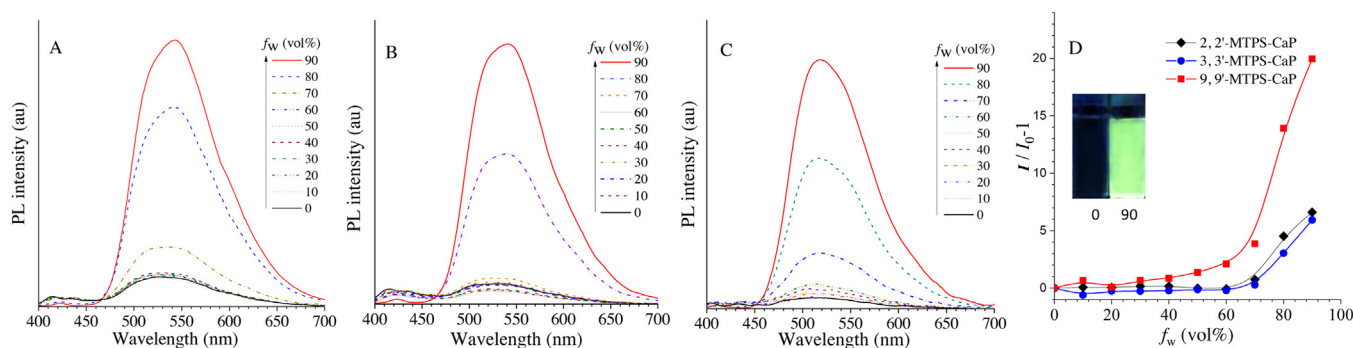
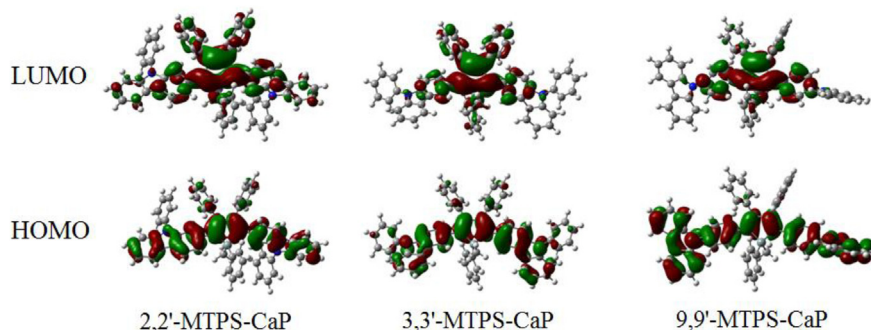


Fig. 1. Molecular structures of these new silole derivatives.

Table 1

Optical properties, thermal stabilities and energy levels of these silole-based luminogens.

Compounds	λ_{abs}^a (nm)	λ_{em} (nm)		Φ_F^c (%)		α_{AIE}^d	T_g/T_d (°C)	HOMO/LUMO ^e (eV)	E_g^f (eV)
		soln ^a	film ^b	soln	film ^a				
2,2'-MTPS-CaP	398	525	539	5.75	69.93	12.16	133.4/433.8	−5.20/−2.70	2.50
3,3'-MTPS-CaP	404	526	531	4.00	60.33	15.08	147.1/452.4	−5.04/−2.49	2.55
9,9'-MTPS-CaP	385	520	520	3.20	80.00	25.00	136.2/440.8	−5.34/−2.62	2.72

^a In THF solution (10^{-5} mol/L).^b Drop-casted film on quartz plate.^c Fluorescence quantum yield, determined by a calibrated integrating sphere.^d Values of AIE effect, calculated by $\Phi_F(\text{film})/\Phi_F(\text{soln})$.^e Determined by CV measurement in solutions.^f Energy band gaps, $E_g = [\text{LUMO} - \text{HOMO}]$ eV.**Fig. 4.** Photoluminescence (PL) spectra of (A) 2,2'-MTPS-CaP, (B) 3,3'-MTPS-CaP and (C) 9,9'-MTPS-CaP in THF/water mixtures with different water fractions (f_w), and (D) plots of $(I/I_0 - 1)$ correspond to different water fractions (f_w), where I_0 is the PL intensity when $f_w = 0\%$, I is the PL intensity in each THF/water mixture ($f_w = 0\text{--}90\%$).**Fig. 5.** The molecular orbital amplitude plots and energy levels of HOMOs and LUMOs of these new silole derivatives, calculated by B3LYP/6-31G(d, p).

their fluorescent nature. The Φ_F and τ can be determined by radiative decay rate (k_r) and nonradiative decay rate (k_{nr}) [12]. Thus, the decay rates of 2,2'-MTPS-CaP, 3,3'-MTPS-CaP and 9,9'-MTPS-CaP had been calculated, including in solution and solid states (Table S1 in Supporting information). For these silole derivatives, once fabricated into solid films, there are great increases in their Φ_F and τ , but small increases in k_r . However, the k_{nr} is decreased significantly. These results manifest that the RIM is triggered in the aggregated state, which blocks the nonradiative decay channel, and thus boosts the PL emissions.

In order to gain an in-depth insight into their AIE property of these silole-based luminogens, their PL spectra in THF/water mixtures were measured and the results are shown in Fig. 4. Since they are insoluble in water, their PL intensity was increased along with the increase of water fraction (f_w) in the mixture. Strong PL emissions were observed in the aggregated state with a high water fraction ($f_w = 90\%$), further validating the AIE property of these silole derivatives.

To investigate the electronic structures of these new silole derivatives, their highest occupied molecular orbitals (HOMOs) and lowest unoccupied molecular orbitals (LUMOs) were calculated by density function theory (DFT) calculation using a B3LYP/6-31G(d, p) basis set on the Gaussian 09 program. The optimized structures and spatial distributions of HOMOs and LUMOs for 2,2'-MTPS-CaP, 3,3'-MTPS-CaP and 9,9'-MTPS-CaP are illustrated in Fig. 5. The HOMOs are located on the entire molecular backbones consisting of central silole ring and carbazole substituents. Their LUMOs, however, are mainly concentrated on the silole ring. The exocyclic single bonds at the 1,1-positions also contribute to the LUMOs, indicative of the unique $\sigma^* - \pi^*$ conjugation.

In order to get the experimental HOMO and LUMO energy levels of these novel silole-based luminogens, the electrochemical properties were investigated by cyclic voltammetry (CV) in dichloromethane solution containing 0.1 mol/L tetra-*n*-butylammonium hexafluorophosphate at a scan rate of 100 mV/s. The working electrode was platinum and the reference electrode was

Ag/AgNO₃ electrode. They showed a good electrochemical stability with reversible oxidation processes (Fig. 6). The values of $E_{\text{onset}}^{\text{ox}}$ and $E_{\text{onset}}^{\text{re}}$ were represented by the onset oxidation and reduction potentials relative to Fc/Fc⁺. The onset potentials of oxidation ($E_{\text{onset}}^{\text{ox}}$) of 2,2'-MTPS-CaP, 3,3'-MTPS-CaP and 9,9'-MTPS-CaP occurred at 0.68, 0.51 and 0.82 V, respectively. Thus, the HOMO energy levels can be determined as -5.20, -5.04 and -5.34 eV, respectively, according to the equation [$\text{HOMO} = -(E_{\text{onset}}^{\text{ox}} + 4.8)$ eV]. While the onset potentials of reduction ($E_{\text{onset}}^{\text{re}}$) of these silole derivatives occurred at -1.92, -2.21 and -2.09 V, respectively, and their LUMO energy levels were calculated to be -2.70, -2.49 and -2.62 eV, respectively, from the equation [$\text{LUMO} = -(E_{\text{onset}}^{\text{re}} + 4.8)$ eV]. The variation tendency of energy band gaps between HOMOs and LUMOs are consistent with optical band gaps (E_g) (Table 1).

Given the high solid-state emission efficiency and favorable thermal stability of these new silole derivatives, their potentials as

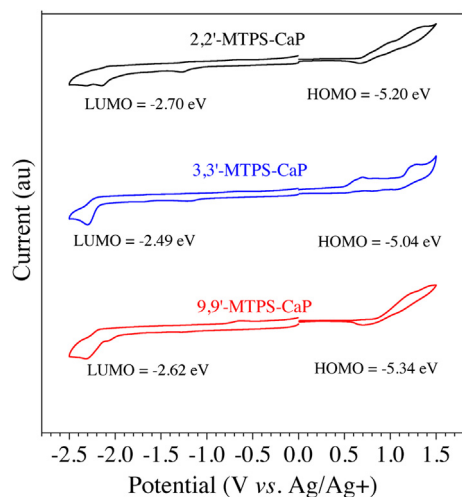


Fig. 6. Cyclic voltammograms of the films of 2,2'-MTPS-CaP, 3,3'-MTPS-CaP, 9,9'-MTPS-CaP, measured in acetonitrile containing 0.1 mol/L tetra-*n*-butylammonium hexafluorophosphate. Scan rate: 100 mV/s.

light-emitting layers in non-doped OLEDs were evaluated. The non-doped OLEDs with a configuration of ITO/NPB (60 nm)/emitter (20 nm)/TPBi (40 nm)/LiF (1 nm)/Al were fabricated, in which new silole derivatives worked as light-emitting layers, NPB (*N,N'*-di(1-naphthyl)-*N,N'*-diphenyl-benzidine) functioned as the hole-transporting layer, and TPBi (1,3,5-tri(1-phenylbenzimidazol-2-yl)-benzene) served as the electron-transporting layer. The EL performance data for the non-doped OLEDs based on these silole derivatives are shown in Fig. 7 and Table 2. These non-doped OLEDs could be turned on at voltages of 2.9–5.3 V, and radiated green lights. The maxima EL peaks of 2,2'-MTPS-CaP, 3,3'-MTPS-CaP and 9,9'-MTPS-CaP are located at 555 (CIE_{x,y} = 0.244, 0.435), 552 (CIE_{x,y} = 0.399, 0.559) and 542 nm (CIE_{x,y} = 0.376, 0.549), respectively, which are red-shifted by 16–22 nm in comparison with the PL emissions in films. Actually, this is a common phenomenon for the luminescent materials because of the microcavity effect [13]. The devices of 2,2'-MTPS-CaP and 3,3'-MTPS-CaP showed comparable EL performances, with maxima luminance ($\eta_{\text{L,max}}$) of 83,870 and 78,780 cd/m², maxima current efficiencies ($\eta_{\text{C,max}}$) of 12.72 and 12.44 cd/A, maxima power efficiencies ($\eta_{\text{P,max}}$) of 9.87 and 10.64 lm/W and maxima external quantum efficiencies ($\eta_{\text{ext,max}}$) of 4.01 and 3.57%, respectively. The device of 9,9'-MTPS-CaP exhibited the best EL performance, affording high $\eta_{\text{L,max}}$, $\eta_{\text{C,max}}$, $\eta_{\text{P,max}}$ and $\eta_{\text{ext,max}}$ of 91,920 cd/m², 17.59 cd/A, 12.55 lm/W, and 5.63%, respectively. The excellent $\eta_{\text{ext,max}}$ is actually approaching the theoretical efficiency limit of fluorescent OLEDs.

In summary, a series of new silole derivatives functionalized by carbazole groups had been synthesized and characterized successfully. All of these new silole derivatives showed good thermal and electrochemical stabilities. They exhibited prominent AIE properties with high Φ_{F} s in the solid state. Different connection pattern between silole and carbazole groups resulted in slightly varied optical properties. Efficient non-doped OLEDs based on these silole derivatives were fabricated. The device of 9,9'-MTPS-CaP afforded the best EL performance, with excellent $\eta_{\text{L,max}}$, $\eta_{\text{C,max}}$, $\eta_{\text{P,max}}$ and $\eta_{\text{ext,max}}$ of 91,920 cd/m², 17.59 cd/A, 12.55 lm/W, and 5.63%, respectively, indicating the good potential for the application in OLEDs.

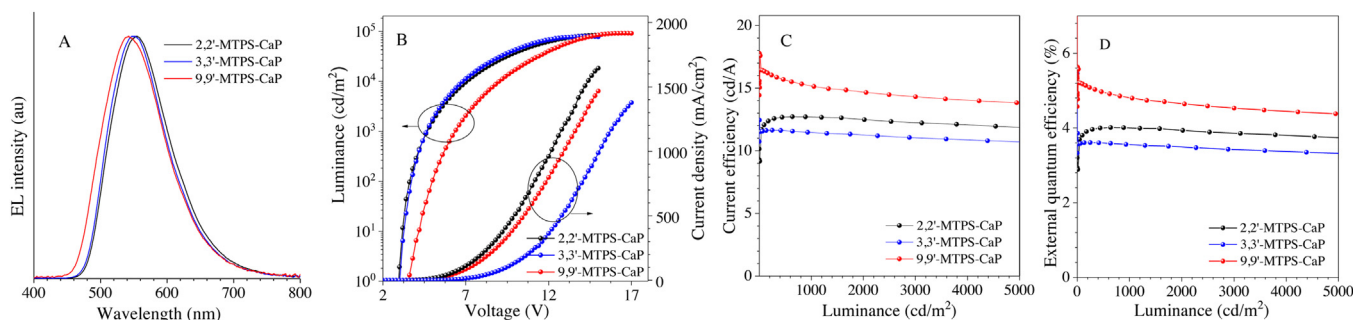


Fig. 7. (A) EL spectra, (B) current density-voltage-luminance, (C) current and (D) external quantum efficiencies with the luminance of the non-doped OLEDs based on 2,2'-MTPS-CaP, 3,3'-MTPS-CaP and 9,9'-MTPS-CaP.

Table 2

EL performances of OLEDs based on these silole derivatives.^a

Emitters	λ_{EL} (nm)	V_{on} (V)	L_{max} (cd/m ²)	$\eta_{\text{C,max}}$ (cd/A)	$\eta_{\text{P,max}}$ (lm/W)	$\eta_{\text{ext,max}}$ (%)	CIE (x, y)
2,2'-MTPS-CaP	555	2.9	83,870	12.72	9.87	4.01	(0.244, 0.435)
3,3'-MTPS-CaP	552	3.1	78,780	12.44	10.64	3.57	(0.399, 0.559)
9,9'-MTPS-CaP	542	5.3	91,920	17.59	12.55	5.63	(0.376, 0.549)

^a The maximum luminescence (L_{max}), maximum current efficiency ($\eta_{\text{C,max}}$), maximum power efficiency ($\eta_{\text{P,max}}$) and the maximum external quantum efficiency ($\eta_{\text{ext,max}}$) of the devices; V_{on} is the turn-on voltage at 1 cd/m² and CIE coordinates at 100 mA/cm².

Acknowledgments

This work was financially supported by the National Natural Science Foundation of China (Nos. 21788102 and 21673082), the National Basic Research Program of China (973 Program, No. 2015CB655004) founded by MOST, the Guangdong Natural Science Funds for Distinguished Young Scholar (No. 2014A030306035), the Science and Technology Program of Guangzhou (No. 201804020027), International Science and Technology Cooperation Program of Guangzhou (No. 201704030069) and the Innovation and Technology Commission of Hong Kong (No. ITC-CNERC14SC01).

Appendix A. Supplementary data

Supplementary material related to this article can be found, in the online version, at doi:<https://doi.org/10.1016/j.ccllet.2018.12.020>.

References

- [1] (a) W. Tang, A. VanSlyke, *Appl. Phys. Lett.* 51 (1987) 913–915;
(b) H. Sasabe, J. Kido, *J. Mater. Chem. C* 1 (2013) 1699–1707.
- [2] (a) H. Chen, J. Lee, B. Lin, et al., *Sci. Appl.* (2018) 17168–17180;
(b) M.C. Gather, A. Köhnen, K. Meerholz, *Adv. Mater.* 23 (2011) 233–248.
- [3] (a) B. Chen, B. Liu, J. Zeng, et al., *Adv. Funct. Mater.* 28 (2018) 1803369;
(b) H. Liu, J. Zeng, J. Guo, et al., *Angew. Chem. Int. Ed.* 57 (2018) 9290–9294.
- [4] (a) B.B. John, *Photophysics of Aromatic Molecule*, Wiley-Interscience, London, New York, 1970, pp. 1–704;
(b) L. Chen, S. Xu, M. Duncan, et al., *Am. Chem. Soc.* 122 (2000) 9302–9303.
- [5] J. Wang, Y. Zhao, C. Dou, et al., *J. Phys. Chem. B* 111 (2011) 5082–5089.
- [6] (a) B.Z. Tang, X. Zhan, G. Yu, et al., *J. Mater. Chem.* 11 (2011) 2974–2978;
(b) J. Luo, Z. Xie, J.W.Y. Lam, et al., *Chem. Commun.* (2001) 1740–1741;
(c) Z. Zhao, J.W.Y. Lam, B.Z. Tang, et al., *Mater. Chem.* 22 (2012) 23726–23740;
(d) Z. Zhao, J.W.Y. Lam, C.Y.K. Chan, et al., *Adv. Mater.* 23 (2011) 5430–5435;
(e) Z. Zhao, S. Chen, J.W.Y. Lam, et al., *Chem. Commun.* 46 (2010) 2221–2223.
- [7] (a) J. Mei, Y. Hong, J.W.Y. Lam, et al., *Adv. Mater.* 26 (2014) 5429–5479;
(b) W. Guan, W. Zhou, C. Lu, et al., *Angew. Chem. Int. Ed.* 54 (2015) 15160–15164;
(c) J. Mei, N.L.C. Leung, R.T.K. Kwok, et al., *Chem. Rev.* 21 (2015) 11718–11940;
(d) T. Zhang, Q. Peng, C. Quan, et al., *Chem. Sci.* 7 (2016) 5573–5580.
- [8] Z. Zhao, P. Lu, J.W.Y. Lam, et al., *Chem. Sci.* 2 (2011) 672–675.
- [9] (a) Z. Zhao, B. He, B.Z. Tang, *Chem. Sci.* 6 (2015) 5347–5365;
(b) P. Shen, Z. Zhuang, Z. Zhao, et al., *J. Mater. Chem. C* 6 (2018) 11835–11852;
(c) J. Yang, N. Sun, J. Huang, et al., *J. Mater. Chem. C* 3 (2015) 2624–2631;
(d) P. Ajay, F. Hendrik, Y.G. Nir, et al., *Adv. Mater.* 27 (2015) 93–100;
(e) S. Yin, Y. Yi, Q. Li, et al., *J. Phys. Chem. A* 110 (2006) 7138–7143.
- [10] (a) T. Jiang, Y. Jiang, W. Qin, et al., *J. Mater. Chem.* 22 (2012) 20266–20272;
(b) L. Chen, Y. Jiang, H. Nie, et al., *Adv. Funct. Mater.* 24 (2014) 3621–3630;
(c) B. Chen, Y. Jiang, B. He, et al., *Chem. Eur. J.* 20 (2014) 1931–1939;
(d) C. Quan, H. Nie, R. Hu, et al., *Chin. J. Chem.* 33 (2015) 842–846;
(e) B. Chen, H. Nie, R. Hu, et al., *Sci. China Chem.* 59 (2016) 699–706;
(f) G. Lin, L. Chen, H. Peng, et al., *J. Mater. Chem. C* 5 (2017) 4867–4874.
- [11] (a) Z. Zhao, S. Chen, J.W.Y. Lam, et al., *J. Phys. Chem. C* 114 (2010) 7963–7972;
(b) Z. Zhao, S. Chen, X. Shen, et al., *Chem. Commun.* 46 (2010) 686–688.
- [12] (a) G. Yu, S. Yin, Y. Liu, et al., *J. Am. Chem. Soc.* 127 (2005) 6335–6346;
(b) Y. Xie, T. Zhang, Z. Li, et al., *Chem.-Asian J.* 10 (2015) 2154–2161;
(c) H. Nie, C. Chen, J. Zeng, et al., *J. Mater. Chem. C* 6 (2018) 3690–3698.
- [13] G. Lin, H. Peng, L. Chen, et al., *ACS Appl. Mater. Interfaces* 8 (2016) 16799–16808.